

Published in final edited form as:

Eur J Nucl Med Mol Imaging. 2014 June ; 41(6): 1199–1209. doi:10.1007/s00259-013-2678-2.

^{18}F -FLT and ^{18}F -FDOPA PET Kinetics in Recurrent Brain Tumors

Mirwais Wardak¹, Christiaan Schiepers¹, Timothy F. Cloughesy², Magnus Dahlbom¹, Michael E. Phelps¹, and Sung-Cheng Huang^{1,*}

¹Department of Molecular and Medical Pharmacology, David Geffen School of Medicine at UCLA, Los Angeles, California

²Department of Neurology, David Geffen School of Medicine at UCLA, Los Angeles, California

Abstract

Purpose—In this study, kinetic parameters of the cellular proliferation tracer ^{18}F -3'-deoxy-3'-fluoro-L-thymidine (FLT) and the amino acid probe 3,4-dihydroxy-6- ^{18}F -fluoro-L-phenylalanine (FDOPA) were measured before and early after the start of therapy, and were used to predict the overall survival (OS) of patients with recurrent malignant glioma using multiple linear regression (MLR) analysis.

Methods—High-grade recurrent brain tumors were investigated in 21 patients (11 male and 10 female; ages 26–76 years). For both probes, each patient had 3 dynamic PET studies: at baseline and after 2 and 6 weeks from the start of treatment. Treatment consisted of biweekly cycles of bevacizumab (an angiogenesis inhibitor) and irinotecan (a chemotherapeutic agent). At each study, ~3.5 mCi of FLT (or FDOPA) was administered intravenously and dynamic PET images were acquired for 1 hr (or 35 min for FDOPA). A total of 126 PET scans were analyzed. A three-compartment, two-tissue model was applied to estimate tumor FLT and FDOPA kinetic rate constants using a metabolite- and partial volume-corrected input function. MLR analysis was used to model OS as a function of FLT and FDOPA kinetic parameters at each of the 3 studies as well as their relative changes between studies. An exhaustive search of MLR models using three or fewer predictor variables was performed to find the best models.

Results—Kinetic parameters from FLT were more predictive of OS than those from FDOPA. Using information from both probes resulted in a better three-predictor MLR model (adjusted $R^2 = 0.83$) than using information from FDOPA alone (adjusted $R^2 = 0.41$), and only marginally different from using information from FLT alone (adjusted $R^2 = 0.82$). Standardized uptake values (either from FLT alone, FDOPA alone, or both together) gave inferior predictive results (best adjusted $R^2 = 0.25$).

Conclusions—For recurrent malignant glioma treated with bevacizumab and irinotecan, FLT kinetic parameters taken early after the start of treatment (absolute values and their associated changes) can provide sufficient information to predict OS with reasonable confidence using MLR.

*For correspondence or reprints contact: Dr. Sung-Cheng Huang, Department of Molecular and Medical Pharmacology, David Geffen School of Medicine at UCLA, B2-085H CHS, 10833 Le Conte Ave, Los Angeles, CA 90095-6948, Telephone: (310) 825-6647, Fax: (310) 825-4517, hhuang@mednet.ucla.edu.

CONFLICT OF INTEREST

The authors declare that they have no conflict of interest.

The slight increase in accuracy for predicting OS with a combination of FLT and FDOPA PET information may not warrant the additional acquisition of FDOPA PET for therapy monitoring in recurrent glioma patients.

Keywords

Positron Emission Tomography; FLT; FDOPA; Recurrent Glioma; Multiple Linear Regression; Tracer Kinetic Modeling; Treatment Response Assessment; Predictive Biomarkers

INTRODUCTION

In the United States, an estimated 69,720 new cases of primary brain and central nervous system tumors are expected to be diagnosed in 2013 [1]. At least one-third of these tumors will be malignant and associated with a high mortality rate, especially among patients diagnosed with a glioblastoma [1, 2]. Gliomas, which are tumors that arise in the glial cells of the brain, account for approximately 30% of all primary brain and other central nervous system tumors, and 80% of those that are malignant tumors [1]. Glioblastoma accounts for the majority of gliomas and is the most frequent malignant primary brain tumor in adults [1]. The life expectancy of a patient diagnosed with glioblastoma remains 12 to 14 months, only slightly better than it was a century ago [3]. With such a poor prognosis, the ability to accurately predict treatment failure early during therapy would have immense value in clinical practice. Information from imaging technologies can play an important role in this effort.

Magnetic resonance imaging (MRI) is currently the modality of choice for diagnosing and monitoring brain tumors [4]. MRI, however, is not without its pitfalls. The ability of MRI to differentiate between treatment-induced changes and residual or recurrent tumor is limited [5, 6]. The determination of treatment response with MRI can also be difficult, especially after radiochemotherapy or antiangiogenic therapy [7]. It is in these and other areas that the power of functional information from positron emission tomography (PET) can help.

PET is a powerful, non-invasive imaging technique used to visualize and quantify various biochemical and physiological processes in living subjects [8–15]. The temporal resolution and high sensitivity of a PET scanner permits external measurements of the tracer kinetics in tissue over time. When utilized with an appropriate tracer compartmental model, regional tissue function such as blood flow, membrane transport, substrate metabolism, enzyme activity, and receptor-ligand interactions can be quantified [9, 16, 17].

Several PET tracers have been used to study various aspects of brain tumor metabolism [15, 18–21]. Among them are 2-deoxy-2-¹⁸F-fluoro-D-glucose (FDG) for imaging glucose uptake, 3'-deoxy-3'-¹⁸F-fluorothymidine (FLT) for imaging cellular proliferation, and 3,4-dihydroxy-6-¹⁸F-fluoro-L-phenylalanine (FDOPA) for imaging amino acid transport. Despite the utility of FDG PET for brain tumor imaging, there are also some limitations [22, 23]. For example, due to the high physiologic glucose metabolism of normal gray matter, the detectability of tumors with only modest increases in glucose metabolism, such as in low-grade tumors and in some cases recurrent high-grade tumors, has proved to be difficult [24]. In addition, the specificity of FDG in tumor detection is sometimes limited by uptake in

non-tumor regions of inflammation and at previous tumor sites exhibiting residual inflammation [25]. FLT PET, on the other hand, has been shown to be more sensitive than FDG for detecting recurrent high-grade brain tumors (likely due to the low background uptake of FLT in normal brain tissue), correlated better with the *ex vivo* Ki-67 proliferation marker, and was a more powerful predictor of tumor progression and survival than FDG PET [26]. FLT PET has also been shown to be more predictive than MRI for early treatment response in recurrent malignant glioma [5].

FDOPA PET offers the advantage of detecting primary and recurrent brain tumors (both high- and low-grade), and its uptake correlates with the grade of newly diagnosed glioma [6, 27]. The transport of FDOPA also does not depend on a breakdown of the blood-brain barrier (BBB) [6, 24]. In head-to-head comparisons, FDOPA was shown to be more accurate than FDG for imaging low-grade tumors and evaluating recurrent tumors [28]. It was also found that FDOPA PET might prove especially useful for distinguishing tumor recurrence from radiation necrosis [28].

Our group at UCLA has previously shown that in patients with recurrent glioma on bevacizumab and irinotecan therapy, relative changes in FLT kinetic parameters (before and early after the start of treatment) were able to correctly classify patients into one of two groups: those that lived less than 1 year and those that lived greater than or equal to 1 year [29]. In this study, 21 patients with recurrent high-grade glioma were given both FLT and FDOPA at baseline and at two time points early after the start of therapy. FLT and FDOPA kinetic parameters were then estimated and used to predict each patient's overall survival (OS) using multiple linear regression (MLR) analysis. It was hypothesized that parameters from both probes together would provide better predictive results than either one alone.

MATERIALS AND METHODS

Patients

Twenty-one patients with recurrent high-grade glioma were investigated in this study. There were 11 men and 10 women, with a median age of 59 y at the start of the study (range: 26–76 y). All gliomas were confirmed by histopathology and graded according to the World Health Organization scheme. Twenty patients had glioblastoma multiforme (GBM; grade IV) and one patient had anaplastic astrocytoma (AA; grade III). Inclusion/exclusion criteria included adult patients (18 years and older) with recurrent malignant glioma with prior surgery and at least one therapeutic failure from chemoradiation, radiation or chemotherapy; pathologic evidence of malignant glioma; tumor progression confirmed by MRI with a contrast enhancing lesion that was measurable; Karnofsky performance status at, or above 60%; adequate blood counts, liver function, kidney function, electrolytes; and no evidence of other serious medical problem. Patients were also selected based upon their perceived likelihood of completing the imaging schedule. Written informed consent was obtained from all patients in accordance with the procedures of the Office of the Human Research Protection Program at UCLA. An overview of the population data is shown in Table 1.

Treatment

Treatment consisted of biweekly cycles of bevacizumab (Avastin; Genentech) and irinotecan (Camptosar; Pfizer). Bevacizumab is a full-length recombinant humanized monoclonal antibody that was designed to bind and inhibit the vascular endothelial growth factor. It was given accelerated approval by the U.S. Food and Drug Administration in May 2009 for the treatment of recurrent GBM. Irinotecan is a prodrug that is converted by esterases (primarily in the liver) to its more potent phenolic form, SN-38. Both the parent drug and SN-38 can bind to topoisomerase I after it complexes with DNA, preventing repair of single-strand breaks caused by topoisomerase I. This complex of irinotecan or SN-38 with the topoisomerase and DNA is cytotoxic to the cell, which is both its therapeutic mechanism of action and the mechanism of action for its toxicity [30]. Treatment with both agents continued until the patient experienced any signs of clinical or radiographic disease progression. All 21 enrolled patients finished the first course of 6 weeks. No patient was lost to follow-up.

Outcome Measurements

Patients had regular follow-up at the UCLA Neuro-Oncology Clinic, and the date of progression was diagnosed by the neuro-oncologist on the basis of physical examination, clinical evaluation, and imaging. Each patient's disease status was evaluated and monitored using gadolinium-enhanced and non-enhanced MRI within 1 week before and at approximately 6-week intervals after the start of treatment. Progression-free survival (PFS) was calculated from the date of baseline FLT PET to the date of disease progression. OS was calculated from the date of baseline FLT PET to the date of patient death. All patients were followed until death.

FLT and FDOPA Synthesis

The chemical structures of FLT and FDOPA are shown in Supplementary Figure S1. FLT was synthesized according to the method developed by Walsh and colleagues [31]. FDOPA was synthesized according to the procedure pioneered by Barrio and colleagues [32]. The specific activity for FLT was more than 1,000 Ci/mmol, while the specific activity for FDOPA was 1–5 Ci/mmol. The maximum radiochemical yield for FLT and FDOPA was approximately 30% and 25%, respectively. The chemical and radiochemical purities for both imaging agents were more than 99%. The final products were sterile and pyrogen free.

Imaging Protocol

For each patient, baseline FLT and FDOPA PET scans [study 1 (S1)] were carried out within 1 week before the start of treatment, and follow-up FLT and FDOPA PET scans were carried out at 2 weeks [study 2 (S2)] and then again at 6 weeks [study 3 (S3)] after the start of treatment (Figure 1). A total of 126 PET scans were analyzed. PET imaging was carried out with an ECAT EXACT HR+ scanner (Siemens/CTI). The intrinsic spatial resolution of the scanner was 4.5 mm in full-width at half-maximum (FWHM) in the center of the field of view. Using a set of external rotating $^{68}\text{Ge}/^{68}\text{Ga}$ rod sources, a transmission scan was first acquired for 5 minutes in 2-dimensional mode to correct for photon attenuation. Shortly thereafter, approximately 3.5 mCi of FLT (or FDOPA) was administered intravenously as a

bolus, and dynamic PET images were acquired in 3-dimensional mode for 1 hour (or 35 minutes for FDOPA).

The emission scan was reconstructed with iterative techniques using the maximum likelihood expectation maximization algorithm accelerated with ordered subsets [33, 34]. After the reconstruction step, the image was smoothed with a 3-dimensional Gaussian filter (FWHM = 4 mm). The final reconstructed PET image had a spatial resolution of 6.0 mm in FWHM and was composed of an image matrix that consisted of $128 \times 128 \times 63$ voxels, with each voxel having near isotropic dimensions ($2.41 \times 2.41 \times 2.43 \text{ mm}^3$). The study protocol was approved by the UCLA Institutional Review Board, the UCLA Medical Radiation Safety Committee, and the UCLA Radioactive Drug Research Committee.

Factor Analysis

Factor analysis (FA) is a data-driven technique that identifies the predominant kinetic patterns present in a dynamic study [35–38]. In our implementation, 3 factor images (representing the brain vessels, tumor, and the rest) were generated. A 50% threshold on the vascular factor image was used to create a volume-of-interest (VOI) that would extract the blood time-activity curve (TAC) when overlaid on the dynamic PET image [39]. The vascular VOI was constrained to the posterior part of the brain, where the transverse sinuses are located. Small blood vessels were explicitly excluded during the thresholding process as they would have a much larger partial volume effect. Similarly, the tumor TAC was extracted with a 75% threshold on the tumor factor image, so as to capture the most active part of the tumor while excluding any necrotic zones. The blood and tumor time-activity curves (TACs) were then used for kinetic modeling analysis. It is important to note that the factor TACs themselves were not used in the kinetic modeling analysis but were only calculated to create the factor images. The extraction fraction for FLT and FDOPA in brain tissue was low, and the arterial-venous difference was small; therefore, our input function was a close approximation of the local arterial blood curve.

FLT Compartmental Model

The compartmental model for FLT is shown in Figure 2A. Briefly, the model assumes a transport step of FLT from the vascular space into the tissue space. There is no partitioning in the vascular space, and it has been previously shown that there are no differences in the FLT activity concentrations between plasma and whole blood [40, 41]. In the tissue space, there is an exchangeable compartment (with intact FLT nucleosides) and a compartment with phosphorylated FLT (mono-, di-, and triphosphate FLT nucleotides). The phosphorylated products of FLT are retained in tissue at a rate proportional to thymidine kinase 1 (TK1) activity [40]. TK1 is a cell cycle regulated enzyme with a several fold increased expression during the S phase of the cell cycle [42]. After completion of mitosis, TK1 levels quickly return to basal levels [25]. The up-regulation and down-regulation of TK1 are controlled by distinct regulatory mechanisms [25, 43]. Very few to no FLT nucleotides are incorporated into DNA [39]. FLT can be metabolized by the liver to FLT-glucuronide, which is present only in the vascular space [39]. It is possible for FLT and FLT-glucuronide to cross the red blood cell membrane via generalized nucleoside

transporters [41]. Thymidine is used as the structural blueprint for FLT because it contains the pyrimidine base thymine, which is uniquely incorporated into DNA and not RNA.

Kinetic modeling yields estimates of four rate constants (K_1 , k_2 , k_3 , and k_4) and a fifth parameter, the blood volume (V_b) in tissue. From these five estimated constants, the values of certain physiologically important macro-parameters can be derived. The overall flux of FLT into cells (K_i) is calculated as $K_1 \times k_3 / (k_2 + k_3)$, the volume of distribution (V_d) is calculated as $K_1 / (k_2 + k_3)$, and the phosphorylated fraction (PF) is calculated as $k_3 / (k_2 + k_3)$. The PF is the fraction of FLT transported via K_1 that ends up in the phosphorylated FLT pool. The dimensions of k_2 , k_3 , and k_4 are min^{-1} , K_1 and K_i have units of $\text{mL} \cdot \text{cm}^{-3} \cdot \text{min}^{-1}$, V_b and V_d are in $\text{mL} \cdot \text{cm}^{-3}$, and PF is unitless.

FDOPA Compartmental Model

The compartmental model for FDOPA kinetics in brain tumors is shown in Figure 2B. The model was adapted from the classic paper written by Huang *et al.* [44], which focused on FDOPA kinetics in the striatum and cerebellum of normal human subjects. In brief, the model assumes transport of FDOPA from the vascular space into the tissue space. FDOPA is transported between plasma and tissue through membrane channels specific for large neutral amino acids [45]. In the tissue space, there is an exchangeable compartment and a sequestered compartment. In addition, FDOPA is converted by catechol-O-methyl transferase (COMT) in the peripheral tissues (e.g., liver, kidneys, and lungs) to L-3,4-dihydroxy-6-fluoro-3-O-methylphenylalanine (OMFD), which can cross the BBB bidirectionally [46]. Metabolism of FDOPA to OMFD inside the brain has been demonstrated to be negligible [44]. In the striatum, FDOPA is converted to 6-fluorodopamine (FDA) by the enzyme aromatic amino acid decarboxylase (AAAD), which is represented by the third compartment. Whereas the third compartment is well defined for the striatum (caudate and putamen), it is unclear for tumors [45].

Kinetic modeling with three compartments yields estimates of four rate constants (K_1 , k_2 , k_3 , and k_4) from which the influx rate constant K_1 , V_d , and sequestration fraction (SF) can be calculated. The SF is the fraction of FDOPA transported via K_1 that is sequestered in the amino acid pool of the tumor, which is larger in tumors than in normal tissue. The blood volume in tissue can be estimated as a fifth parameter.

Standardized Uptake Value Measurements

Standardized uptake value (SUV) is a semi-quantitative index that is calculated by normalizing the measured tissue activity concentration to the patient's body weight and injected dose [47]. SUV was calculated at both early and late time points in this study. For FLT, SUV-early and SUV-late were measured from 10–20 and 50–60 minutes, respectively. For FDOPA, SUV-early and SUV-late were measured from 10–20 and 25–35 minutes, respectively.

Metabolite and Partial Volume Corrections

In the present study, no metabolites of FLT and FDOPA were measured in blood. Instead, theoretical curves were fitted to FLT and FDOPA metabolite data that were pooled from

previous publications [40, 48, 49]. The fitted curves were then used as an approximation of the expected metabolite fraction over time for each individual's blood curve.

For FLT, the measured metabolite data in lung cancer and colorectal cancer were extracted from previous publications [40, 48]. Because the metabolite data from these two studies appeared similar, they were pooled together and fitted with a theoretical curve, as an approximation of the metabolite fraction over time. The equation of the metabolite fraction for FLT was calculated as $0.42 \times [1 - \exp(-0.029 \times T)]$, where T is the time (in minutes) after injection.

For FDOPA, correcting for metabolites in blood was a little more complicated. OMFD can cross in and out of red blood cells and thus occupies the total blood volume [44, 49]. On the other hand, FDOPA and other ^{18}F labeled metabolites of FDOPA (collectively referred to as METS from here on) do not cross the red blood cell membrane and are confined to the plasma space [44, 49] (see Appendix Figure A1). We extracted the measured metabolite fractions of plasma radioactivity for OMFD and METS from the publication of Huang *et al.* [49] and fitted exponential curves to them (see Appendix Figure A2). Because no plasma samples for FDOPA and its metabolites were assayed, we had to convert the total ^{18}F activity concentration in whole blood (which we measured with PET) to the total FDOPA activity concentration in plasma. It was only after this conversion that we could input the TAC of our authentic FDOPA tracer in plasma into our FDOPA kinetic model (see Appendix Figure A3). The conversion was done using derived mathematical equations as shown in the Appendix. We used the data by Huang *et al.* [49] because this was the only data found in the literature that measured OMFD and METS in a patient without carbidopa pretreatment, similar to what was done in our study. Carbidopa is a sentry drug that is sometimes given before an FDOPA PET imaging study so that FDA formation is blocked in the peripheral tissues. Carbidopa pretreatment thus increases the bioavailability of FDOPA in plasma.

To address the effects of partial volume, a recovery coefficient of 0.7 was chosen to convert the image-based blood TAC to the input function [39]. Because the tumors were relatively large compared to three times the FWHM of the PET scanner, the recovery coefficient of the output function was set to unity [39].

Statistical Analysis

Multiple linear regression (MLR) was used to model OS as a function of FLT and FDOPA kinetic parameters as well as their associated changes after the start of therapy. In MLR, we attempt to model the relationship between a single outcome variable and two or more explanatory variables by fitting a linear equation to the observed data [50]. It has been recommended that no more than one predictor variable for every five observations should be included in an MLR model [51]. Therefore, we limited our MLR models to three or fewer predictor variables because our sample size ($n = 21$) was relatively small and we did not want to overfit the data. OS was chosen as the outcome variable in the regression analysis because it is the gold standard endpoint for demonstrating clinical efficacy; OS is unequivocal, easily measured and is not subject to investigator interpretation. Furthermore, because measurements were made on the same individual at three different time points, the

Wilcoxon signed-rank test was used to assess whether the median of the differences in the paired data were significantly different from zero. Pearson and Spearman correlations were computed to assess significant associations between OS and the rest of the variables. All statistical analyses were performed using SPSS (version 22; IBM Corporation) and SAS (version 9.4; SAS Institute) software. The results are reported as the mean \pm SD (unless otherwise noted) and are regarded as statistically significant if $P < 0.05$.

RESULTS

Outcome Analysis

Table 1 summarizes the clinical characteristics of the 21 patients. At the time of this writing, all patients had died and therefore all imaging and clinical variables were known. The mean \pm SD of the OS in this sample was 401 ± 252 d (13.2 ± 8.3 months) and the range was 81–1054 d (2.7 months - 2.9 y). The mean \pm SD of PFS was 183 ± 156 d and the range was 42–588 d. The median OS and PFS for the entire sample were 364 days (11.96 months) and 135 days (4.44 months), respectively. Of the patients with a GBM diagnosis at recurrence, 17 patients had a primary (or de novo) GBM and 3 patients had a secondary GBM (i.e., when a low grade glioma transforms into a GBM over time). The mean age of the de novo GBM patients was 58 y, whereas the mean age of the secondary GBM patients was 33 y. In this cohort, OS and PFS were shown to be significantly correlated (Pearson $r = 0.85$, $P < 0.0001$ and Spearman's $\rho = 0.69$, $P < 0.001$).

FLT and FDOPA Data Analysis

Figure 3 shows the vascular and tumor factor images along with their factor analysis-derived blood and tumor TACs. The percent change in FLT and FDOPA kinetic parameters from $S1 \rightarrow S2$, $S1 \rightarrow S3$, and $S2 \rightarrow S3$ are shown in Supplementary Tables S1–S3. The percent change between any two studies could also be written as the ratio of the two studies minus one. For example, $(S2 - S1) / S1$ ($S2 / S1 - 1$), $(S3 - S1) / S1$ ($S3 / S1 - 1$) and $(S3 - S2) / S2$ ($S3 / S2 - 1$). In the MLR analysis, we chose to input only the ratio portion of the percent change (i.e., neglecting the minus one), so that our inputs were greater than zero and not negative; this was done for convenience purposes. Additional information on FLT and FDOPA kinetic parameters at each of the three studies is listed in the Supplementary Materials section (Supplementary Tables S4–S12). Measured and model fitted tumor TACs for sample FLT and FDOPA PET studies are shown in Supplementary Figure S2.

Figure 4A shows FLT PET images for a long-term survivor and two short-term survivors at baseline, and after 2 and 6 weeks from the start of treatment. Figure 4B shows similar images for the same set of patients but with FDOPA PET. Sample FDOPA TACs of the tumor, striatum, and cerebellum at a baseline study are shown in Supplementary Figure S3.

Bar graphs showing the sample mean \pm standard error of the mean (SEM) at each of the three studies for various FLT kinetic and SUV parameters are plotted in Supplementary Figures S4 and S5. For FDOPA, this is shown in Supplementary Figures S6 and S7.

Multiple Linear Regression Analysis

Kinetic parameters from FLT alone provided better results in predicting OS than using information from FDOPA alone (Table 2). Parameters from FLT and FDOPA combined resulted in a better MLR model (adjusted $R^2 = 0.83$) than using information from FDOPA alone (adjusted $R^2 = 0.41$), and not significantly different from using information from FLT alone (adjusted $R^2 = 0.82$). Information from standardized uptake values (either from FLT alone, FDOPA alone, or both together) gave inferior predictive results (best adjusted $R^2 = 0.25$). For each probe, pooling parameter values (at each of the 3 study time points) along with their associated changes between studies resulted in a better regression model than using information provided by them alone (Table 2).

The partial regression coefficients for the MLR models when using information from FLT alone, FDOPA alone, and FLT and FDOPA combined are listed in Table 3 and Supplementary Tables S13 and S14, respectively. All of these models passed various regression diagnostics such as tests for multicollinearity, normality of the residuals, and constant error variance. The predictive results of the best three-parameter MLR model that uses only FLT kinetic information (MLR-1) are shown as scatter plots in Figure 5 and as bar graphs (with error bars) in Supplementary Figure S8A. The root mean square error for the MLR-1 model was 106 days (Table 3). To put the MLR results in perspective, if the sample mean was used for predicting the OS of every patient (and any new patient with a recurrent brain tumor who is undergoing treatment with bevacizumab and irinotecan), then each of these individuals would have a predicted OS of 401 ± 252 days (13.2 ± 8.3 months); with 1 SD, this prediction is anywhere from 149–653 d (4.9–21.5 months) (see Supplementary Figure S8B).

DISCUSSION

To our knowledge, this is the first longitudinal study to investigate and compare both FLT and FDOPA kinetic parameters in patients with recurrent malignant glioma before and early after the start of therapy. In this study, we aimed to develop a multiple linear regression model to predict OS as a continuous variable using information provided to us by two molecular imaging probes. Survival predictions become critical elements in the management of brain tumor patients, especially when the clinical course for glioblastoma is rapid and fatal.

Kinetic analysis with dynamic PET imaging can quantify and capture multiple aspects of tumor biology and their changes in response to treatment. We found that kinetic parameters from FLT alone provided better results in predicting OS than information from FDOPA alone when inputted into an MLR model that used a maximum of three predictor variables. This result seems to agree with findings from previous clinical investigations that were performed separately with FLT and FDOPA PET [27, 52]. Yamamoto *et al.* reported that in patients with recurrent glioma, FLT uptake (calculated as tumor-to-normal ratio) was significantly correlated with tumor proliferative activity [52], as measured by the *ex vivo* Ki-67 tumor proliferation index. The Ki-67 antigen, which is targeted by the MIB-1 antibody, is expressed only in proliferative stages of the cell cycle [24]. Fueger *et al.* found that FDOPA uptake (expressed as SUV) correlated significantly with the Ki-67 tumor

proliferation index in newly diagnosed glioma but not in recurrent glioma [27]. Although FDOPA PET information did not provide great results in predicting the OS of recurrent brain tumor patients using an MLR model, it might still offer other advantages such as capturing the extent of the tumor or for its use in tumor diagnosis.

In this study, parameters from FLT and FDOPA combined resulted in a better MLR model (adjusted $R^2 = 0.83$) than using information from FDOPA alone (adjusted $R^2 = 0.41$), and not markedly different from using information from FLT alone (adjusted $R^2 = 0.82$). This suggests that FLT kinetic parameters taken early after the start of treatment may provide sufficient information to predict OS with reasonable confidence using a multivariate regression analysis. The marginal increase in accuracy for predicting OS with a combination of FLT and FDOPA PET probes may not warrant the additional acquisition of FDOPA PET scans in a clinical setting for therapy monitoring of patients with recurrent malignant glioma. Whether the combined information from FLT and FDOPA PET images may help in the prediction of OS in patients with newly diagnosed glioma remains to be investigated.

The MLR model that used the kinetic information from FLT alone (Table 3) revealed that patients that tended to live longer had a smaller absolute value in their tumor volume of distribution at 2 wks, a larger k_4 ratio from baseline→2 wks, and a larger k_2 ratio from 2 wks→6 wks when compared to short-term survivors. This seems to indicate that, in the tumors of the long-term survivors, the change in the dephosphorylation from baseline→2 wks (right after start of therapy) was more positively increased, the change in the efflux of FLT back into the plasma was more positively increased from 2 wks→6 wks (the rebound phase), and the volume of distribution of the tumor at 2 wks was smaller than that of the short-term survivors. Taken together, these results seem to suggest that the tumors of the long-term survivors may not be cycling through the cell cycle as much as the short-term survivors, or that the tracer goes in and out of the cell without doing anything inside. It must be kept in mind that although TK1 activity is a requirement for the accumulation of FLT, retention is dependent on nucleoside/nucleotide efflux and the retrograde metabolism of FLT nucleotides [53, 54].

The MLR model that used kinetic information from FDOPA alone (Supplementary Table S13) revealed that patients that tended to live longer had a smaller absolute value in their sequestration rate constant k_3 at the baseline study when compared to short-term survivors, a smaller FDOPA tumor volume of distribution at the baseline study when compared to short-term survivors, and a more negative change in their K_1 membrane transport from 2 wks→6 wks (the rebound phase) than the short-term survivors. The relative demand for amino acids was thus generally lower in the tumors of the long-term survivors at baseline (before treatment) and the time period from 2 wks→6 wks, when multiple treatment infusions had already been administered.

In the MLR analysis, PFS was not entered as a possible predictor variable in any of the MLR models because we wanted to use only information available to us at the end of 6 weeks, which, for the most part, was the PET information from the dynamic FLT and FDOPA PET images. We did not want the MLR model to be dependent on the time it took to determine the PFS, which for most patients in our study was more than 6 weeks.

The predictor variables in this study were different from our *Clinical Cancer Research* article [29] because the aims of these two studies were different. In the *Clinical Cancer Research* article [29], we wanted to classify patients into one of two OS groups using discriminant analysis, while in this study we wanted to predict OS as a continuous outcome variable. The number of patients in this study was also larger than our *Clinical Cancer Research* investigation [29].

One of the limitations of this study was that we did not measure metabolite data from the patients but instead used theoretical curves as an approximation of the metabolite fraction over time. This can be a problem if there are fluctuations in the metabolite fraction due to impaired liver function as a result of chemotherapy (i.e., the greater the liver impairment, the more presence of the authentic tracer and the less presence of its metabolic products in plasma). Future work will try to address some of these issues by analyzing the data in a different way. One such approach is to use the reference tissue model [55, 56]. If a brain region can be identified, which is devoid of specific binding, the TAC for this “reference region” can be used as an indirect input function for the target region [57]. An advantage of this method over “classical” compartmental methods is that no metabolite correction is needed [57]. This is because the input function in these simplified reference tissue models can be built into the model itself, utilizing the fact that different tissue regions are exposed to the same input function. Another limitation of this study was the short acquisition time of the FDOPA PET scans (35 min). If we were able to measure out to 75 min, our MLR results for FDOPA may have yielded better predictive results because the shape of the descending portion of the tumor uptake curve can provide additional information [45].

Collectively, this study has demonstrated that the use of PET kinetic analysis and MLR can be a powerful tool for clinicians monitoring patient treatment as it may allow for a window of opportunity during which treatment regimens can be tailored accordingly, depending on the survival predictions from the MLR analysis. Specifically, it offers the neuro-oncologist an index on whether to wait and watch on the current therapy or to switch the patient altogether to a different and potentially more efficacious treatment regimen earlier on. The clinical effect of this added information could potentially help increase patient lifespan, avoid unnecessary drug toxicity to the patient, and reduce undue health care costs. This method could also augment the conventional assessment of tumor response that is done with morphological imaging and could be included in standardized criteria for response evaluation in neuro-oncology. In the meantime, we need clinical chemists to come up with new, more effective, and less toxic therapeutics against this terrible disease. Working on brain tumor research can often be a Herculean task in that fighting against these cancer cells can be like trying to kill the Hydra, which grew back two heads when one was severed. However, we have to persevere like Hercules, and make leaping strides in trying to increase the lifespan of these patients.

Supplementary Material

Refer to Web version on PubMed Central for supplementary material.

Acknowledgments

The authors are grateful to all the patients who participated in this study as well as to their families. In addition, the authors thank David Truong, Dat Vu, and Weber Shao for their computer and database support, the UCLA Cyclotron staff for help with FLT and FDOPA preparation, and the UCLA Nuclear Medicine staff for acquisition of the PET scans. This work was supported by the U.S. Department of Energy contract DEFG02-06ER64249 and NIH grants P50-CA086306 and R01-EB001943.

REFERENCES

1. CBTRUS. Source: Central Brain Tumor Registry of the United States. Hinsdale, IL: 2013. CBTRUS Statistical Report: Primary Brain and Central Nervous System Tumors Diagnosed in the United States in 2005–2009. website: www.cbtrus.org.
2. Siegel R, Naishadham D, Jemal A. Cancer statistics, 2012. *CA Cancer J Clin*. 2012; 62:10–29. [PubMed: 22237781]
3. Foltz G. New Hope For Battling Brain Cancer. *Scientific American Mind*. 2010; 21:50.
4. Clarke JL, Chang SM. Neuroimaging: diagnosis and response assessment in glioblastoma. *Cancer J*. 2012; 18:26–31. [PubMed: 22290254]
5. Schwarzenberg J, Czernin J, Cloughesy TF, Ellingson BM, Pope WB, Geist C, et al. 3'-Deoxy-3'-¹⁸F-Fluorothymidine PET and MRI for Early Survival Predictions in Patients with Recurrent Malignant Glioma Treated with Bevacizumab. *J Nucl Med*. 2012; 53:29–36. [PubMed: 22159180]
6. Walter F, Cloughesy T, Walter MA, Lai A, Nghiemphu P, Wagle N, et al. Impact of 3,4-dihydroxy-6-¹⁸F-fluoro-L-phenylalanine PET/CT on managing patients with brain tumors: the referring physician's perspective. *J Nucl Med*. 2012; 53:393–398. [PubMed: 22323780]
7. Clarke JL, Chang S. Pseudoprogression and pseudoresponse: challenges in brain tumor imaging. *Curr Neurol Neurosci Rep*. 2009; 9:241–246. [PubMed: 19348713]
8. Phelps, ME. PET : molecular imaging and its biological applications. New York: Springer; 2004.
9. Phelps, ME.; Mazziotta, JC.; Schelbert, HR. Positron emission tomography and autoradiography : principles and applications for the brain and heart. New York: Raven Press; 1986.
10. Phelps ME. PET: the merging of biology and imaging into molecular imaging. *J Nucl Med*. 2000; 41:661–681. [PubMed: 10768568]
11. Phelps ME. Positron emission tomography provides molecular imaging of biological processes. *Proceedings of the National Academy of Sciences of the United States of America*. 2000; 97:9226–9233. [PubMed: 10922074]
12. Phelps ME, Huang SC, Hoffman EJ, Selin C, Sokoloff L, Kuhl DE. Tomographic measurement of local cerebral glucose metabolic rate in humans with (F-18)2-fluoro-2-deoxy-D-glucose: validation of method. *Ann Neurol*. 1979; 6:371–388. [PubMed: 117743]
13. Phelps ME, Mazziotta JC. Positron emission tomography: human brain function and biochemistry. *Science*. 1985; 228:799–809. [PubMed: 2860723]
14. Phelps ME, Schelbert HR, Mazziotta JC. Positron computed tomography for studies of myocardial and cerebral function. *Ann Intern Med*. 1983; 98:339–359. [PubMed: 6219602]
15. Weissleder, R. Molecular imaging : principles and practice. Shelton, Conn.: People's Medical Pub. House-USA; 2009.
16. Huang SC, Phelps ME, Hoffman EJ, Sideris K, Selin CJ, Kuhl DE. Noninvasive determination of local cerebral metabolic rate of glucose in man. *Am J Physiol*. 1980; 238:E69–E82. [PubMed: 6965568]
17. Huang SC. Role of Kinetic Modeling in Biomedical Imaging. *J Med Sci*. 2008; 28:57–63. [PubMed: 20640185]
18. Shields AF, Grierson JR, Dohmen BM, Machulla HJ, Stayanoff JC, Lawhorn-Crews JM, et al. Imaging proliferation in vivo with [F-18]FLT and positron emission tomography. *Nature medicine*. 1998; 4:1334–1336.
19. Heiss WD, Wienhard K, Wagner R, Lanfermann H, Thiel A, Herholz K, et al. F-Dopa as an amino acid tracer to detect brain tumors. *J Nucl Med*. 1996; 37:1180–1182. [PubMed: 8965194]

20. Herholz K, Langen KJ, Schiepers C, Mountz JM. Brain tumors. *Seminars in nuclear medicine*. 2012; 42:356–370. [PubMed: 23026359]
21. Heiss WD, Raab P, Lanfermann H. Multimodality assessment of brain tumors and tumor recurrence. *J Nucl Med*. 2011; 52:1585–1600. [PubMed: 21840931]
22. Olivero WC, Dulebohn SC, Lister JR. The use of PET in evaluating patients with primary brain tumours: is it useful? *J Neurol Neurosurg Psychiatry*. 1995; 58:250–252. [PubMed: 7876865]
23. Ricci PE, Karis JP, Heiserman JE, Fram EK, Bice AN, Drayer BP. Differentiating recurrent tumor from radiation necrosis: time for re-evaluation of positron emission tomography? *Am J Neuroradiol*. 1998; 19:407–413. [PubMed: 9541290]
24. Chen W. Clinical applications of PET in brain tumors. *J Nucl Med*. 2007; 48:1468–1481. [PubMed: 17704239]
25. Bading JR, Shields AF. Imaging of cell proliferation: status and prospects. *J Nucl Med*. 2008; 49(Suppl 2):64S–80S. [PubMed: 18523066]
26. Chen W, Cloughesy T, Kamdar N, Satyamurthy N, Bergsneider M, Liau L, et al. Imaging proliferation in brain tumors with ^{18}F -FLT PET: comparison with ^{18}F -FDG. *J Nucl Med*. 2005; 46:945–952. [PubMed: 15937304]
27. Fueger BJ, Czernin J, Cloughesy T, Silverman DH, Geist CL, Walter MA, et al. Correlation of 6- ^{18}F -fluoro-L-dopa PET uptake with proliferation and tumor grade in newly diagnosed and recurrent gliomas. *J Nucl Med*. 2010; 51:1532–1538. [PubMed: 20847166]
28. Chen W, Silverman DH, Delaloye S, Czernin J, Kamdar N, Pope W, et al. ^{18}F -FDOPA PET imaging of brain tumors: comparison study with ^{18}F -FDG PET and evaluation of diagnostic accuracy. *J Nucl Med*. 2006; 47:904–911. [PubMed: 16741298]
29. Wardak M, Schiepers C, Dahlbom M, Cloughesy T, Chen W, Satyamurthy N, et al. Discriminant analysis of ^{18}F -fluorothymidine kinetic parameters to predict survival in patients with recurrent high-grade glioma. *Clin Cancer Res*. 2011; 17:6553–6562. [PubMed: 21868765]
30. Zdanowicz, MM. American Society of Health-System Pharmacists. *Concepts in pharmacogenomics*. Bethesda, MD: American Society of Health-System Pharmacists; 2010.
31. Walsh, JC.; Padgett, HC.; Ysaguirre, T. *Method for preparing radiolabeled thymidine having low chromophoric byproducts*. Siemens Medical Solutions USA, Inc.; 2008.
32. Namavari M, Bishop A, Satyamurthy N, Bida G, Barrio JR. Regioselective radiofluorodestannylation with [^{18}F]F₂ and [^{18}F]CH₃COOF: a high yield synthesis of 6- ^{18}F Fluoro-L-dopa. *Int J Rad Appl Instrum A*. 1992; 43:989–996. [PubMed: 1330984]
33. Hudson HM, Larkin RS. Accelerated image reconstruction using ordered subsets of projection data. *IEEE Trans Med Imaging*. 1994; 13:601–609. [PubMed: 18218538]
34. Nuyts J, Michel C, Dupont P. Maximum-likelihood expectation-maximization reconstruction of sinograms with arbitrary noise distribution using NEC-transformations. *IEEE Trans Med Imaging*. 2001; 20:365–375. [PubMed: 11403196]
35. Schiepers C, Hoh CK, Nuyts J, Wu HM, Phelps ME, Dahlbom M. Factor analysis in prostate cancer: delineation of organ structures and automatic generation of in- and output functions. *IEEE Trans Nucl Sci*. 2002; 49:2338–2343.
36. Schiepers C, Hoh CK, Dahlbom M, Wu HM, Phelps ME. Factor analysis for delineation of organ structures, creation of in- and output functions, and standardization of multicenter kinetic modeling. *Proceedings SPIE*. 1999; 3661:1343–1350.
37. Sitek A, Di Bella EV, Gullberg GT. Factor analysis with a priori knowledge--application in dynamic cardiac SPECT. *Physics in medicine and biology*. 2000; 45:2619–2638. [PubMed: 11008961]
38. Ell, PJ.; Gambhir, SS. *Nuclear medicine in clinical diagnosis and treatment*. 3rd ed.. Edinburgh; New York: Churchill Livingstone; 2004.
39. Schiepers C, Chen W, Dahlbom M, Cloughesy T, Hoh CK, Huang SC. ^{18}F -fluorothymidine kinetics of malignant brain tumors. *Eur J Nucl Med Mol Imaging*. 2007; 34:1003–1011. [PubMed: 17295039]
40. Muzi M, Vesselle H, Grierson JR, Mankoff DA, Schmidt RA, Peterson L, et al. Kinetic analysis of 3'-deoxy-3'-fluorothymidine PET studies: validation studies in patients with lung cancer. *J Nucl Med*. 2005; 46:274–282. [PubMed: 15695787]

41. Personal Communication with Dr. John R. Grierson.
42. Reske SN, Deisenhofer S. Is 3'-deoxy-3'-(18)F-fluorothymidine a better marker for tumour response than (18)F-fluorodeoxyglucose? *Eur J Nucl Med Mol Imaging*. 2006; 33(Suppl 1):38–43. [PubMed: 16721567]
43. Shields AF. PET imaging of tumor growth: not as easy as it looks. *Clin Cancer Res*. 2012; 18:1189–1191. [PubMed: 22275505]
44. Huang SC, Yu DC, Barrio JR, Grafton S, Melega WP, Hoffman JM, et al. Kinetics and modeling of L-6-[¹⁸F]fluoro-dopa in human positron emission tomographic studies. *J Cereb Blood Flow Metab*. 1991; 11:898–913. [PubMed: 1939385]
45. Schiepers C, Chen W, Cloughesy T, Dahlbom M, Huang SC. ¹⁸F-FDOPA kinetics in brain tumors. *J Nucl Med*. 2007; 48:1651–1661. [PubMed: 17873130]
46. Beuthien-Baumann B, Bredow J, Burchert W, Fuchtnner F, Bergmann R, Alheit HD, et al. 3-O-methyl-6-[¹⁸F]fluoro-L-DOPA and its evaluation in brain tumour imaging. *Eur J Nucl Med Mol Imaging*. 2003; 30:1004–1008. [PubMed: 12768333]
47. Huang SC. Anatomy of SUV. Standardized uptake value. *Nucl Med Biol*. 2000; 27:643–646. [PubMed: 11091106]
48. Visvikis D, Francis D, Mulligan R, Costa DC, Croasdale I, Luthra SK, et al. Comparison of methodologies for the in vivo assessment of ¹⁸FLT utilisation in colorectal cancer. *Eur J Nucl Med Mol Imaging*. 2004; 31:169–178. [PubMed: 15129698]
49. Huang SC, Barrio JR, Yu DC, Chen B, Grafton S, Melega WP, et al. Modelling approach for separating blood time-activity curves in positron emission tomographic studies. *Physics in medicine and biology*. 1991; 36:749–761. [PubMed: 1908103]
50. Petrie, A.; Sabin, C. *Medical statistics at a glance*. 3rd ed.. Chichester, UK ; Hoboken, NJ: Wiley-Blackwell; 2009.
51. Dietz, T.; Kalof, L. *Introduction to social statistics : the logic of statistical reasoning*. Chichester, West Sussex ; Malden, MA: Wiley-Blackwell; 2009.
52. Yamamoto Y, Ono Y, Aga F, Kawai N, Kudomi N, Nishiyama Y. Correlation of ¹⁸F-FLT Uptake with Tumor Grade and Ki-67 Immunohistochemistry in Patients with Newly Diagnosed and Recurrent Gliomas. *J Nucl Med*. 2012; 53:1911–1915. [PubMed: 23081994]
53. Plotnik DA, McLaughlin LJ, Chan J, Redmayne-Titley JN, Schwartz JL. The role of nucleoside/nucleotide transport and metabolism in the uptake and retention of 3'-fluoro-3'-deoxythymidine in human B-lymphoblast cells. *Nuclear medicine and biology*. 2011; 38:979–986. [PubMed: 21982569]
54. Grierson JR, Schwartz JL, Muzi M, Jordan R, Krohn KA. Metabolism of 3'-deoxy-3'-[F-18]fluorothymidine in proliferating A549 cells: validations for positron emission tomography. *Nuclear medicine and biology*. 2004; 31:829–837. [PubMed: 15464384]
55. Lammertsma AA, Hume SP. Simplified reference tissue model for PET receptor studies. *Neuroimage*. 1996; 4:153–158. [PubMed: 9345505]
56. Lammertsma AA, Bench CJ, Hume SP, Osman S, Gunn K, Brooks DJ, et al. Comparison of methods for analysis of clinical [¹¹C]raclopride studies. *J Cereb Blood Flow Metab*. 1996; 16:42–52. [PubMed: 8530554]
57. Khalil, MM. *Basic sciences of nuclear medicine*. Heidelberg: Springer; 2011.

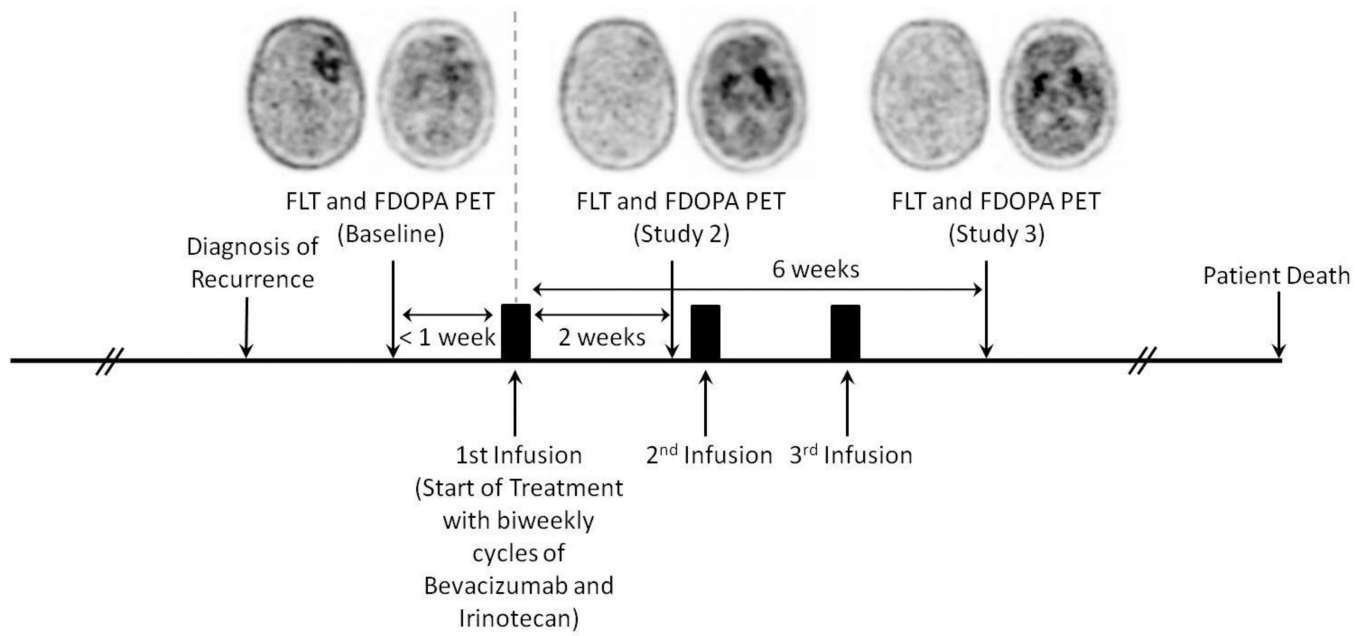


Figure 1.

Experimental design showing the relative timing of treatment administration and PET image acquisition. Each patient was used as his or her own control.

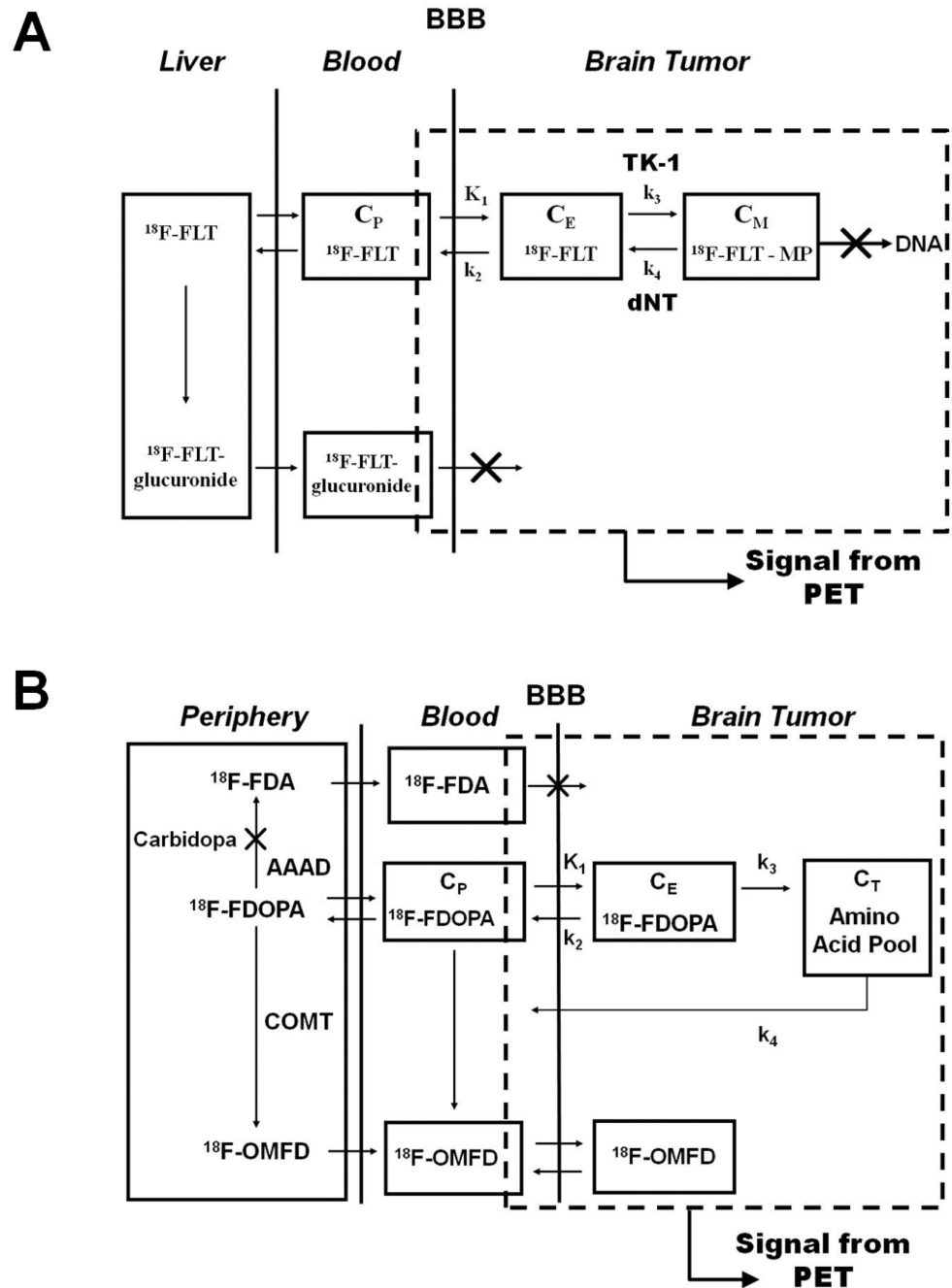


Figure 2.

(A) Tracer kinetic model for FLT in brain tumors. The catenary model consists of a vascular compartment and two tissue compartments, each of which represents FLT in one of two different chemical states. Intracellular radioactivity accumulation results from the formation of phosphorylated FLT nucleotides in competition with nucleotidase-mediated dephosphorylation and FLT efflux [42]. K_1 is the transport rate constant of FLT from blood (or plasma) into the tumor cell via nucleoside-facilitated transporters, k_2 is the loss or leak from the system, k_3 is the rate constant for kinase-modulated phosphorylation of FLT, and k_4 is the rate constant that describes the dephosphorylation of FLT-monophosphate by phosphatases [such as 5' (3')-deoxyribonucleotidase 1 (dNT1)] [42]. (B) Tracer kinetic model for FDOPA in brain tumors. FDOPA is transported across

tumor cell membranes by L-amino acid transporters, which are overexpressed in most gliomas [38]. Increased transport of amino acids is most likely a result of increased demand for amino acids. The parameter k_3 is the sequestration rate constant which describes the transfer of FDOPA into the amino acid pool of the tumor, which is larger in tumors than in normal brain tissue (e.g., cerebral cortex and cerebellum). Huang *et al.* was the first to estimate FDOPA kinetics in the brains of normal human subjects [44]. Schiepers *et al.* was the first to report FDOPA kinetics in human brain tumors [45].

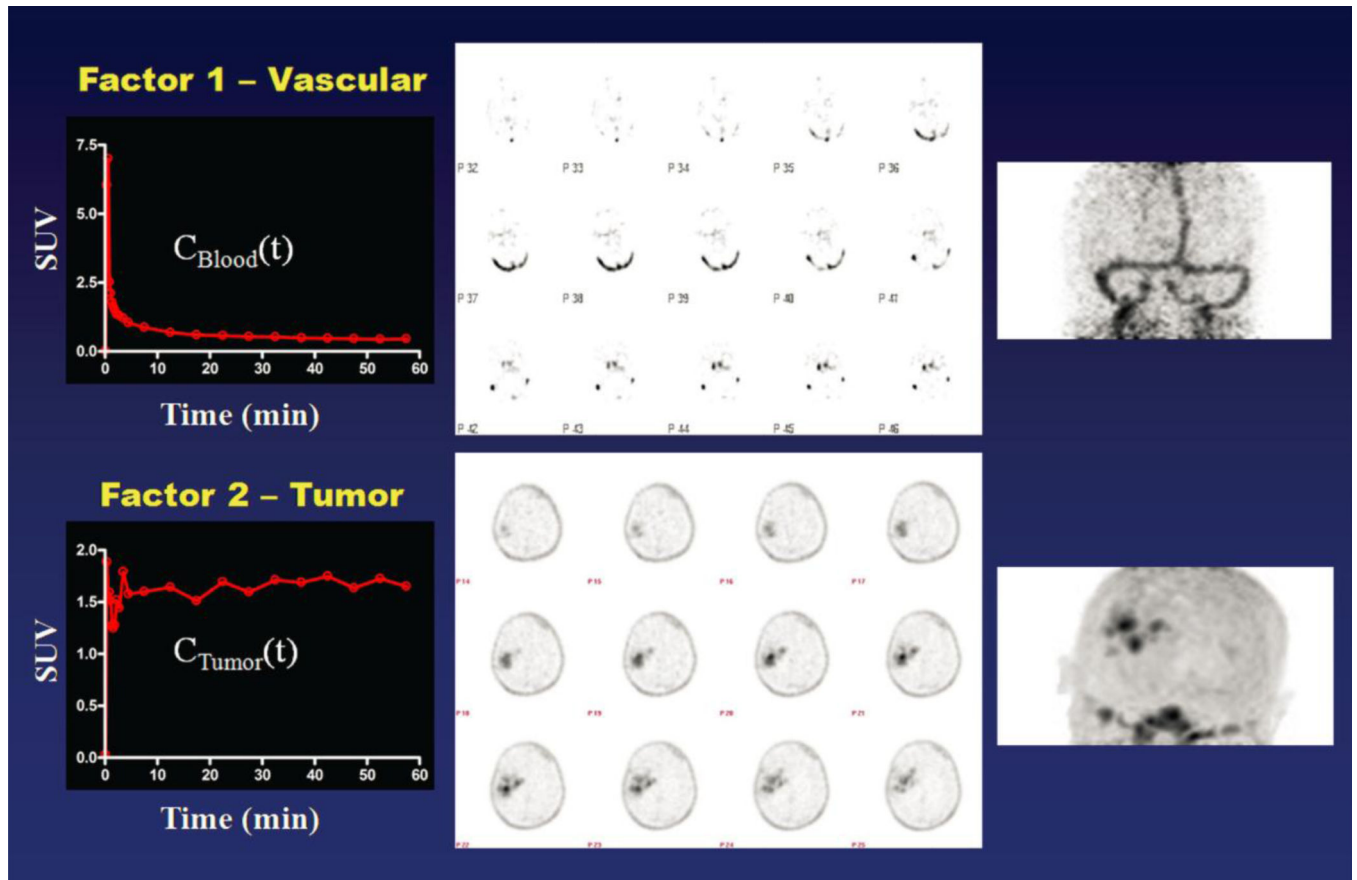


Figure 3.

Vascular and tumor factor images along with their corresponding blood and tumor TACs as shown for an FLT PET study. The superior sagittal sinus and the left and right transverse sinuses can be seen in the vascular factor image. Note the tumor and normal bone marrow in the tumor factor image. This figure nicely illustrates the different types of biological information provided by a dynamic PET scan at early and late times after tracer injection.

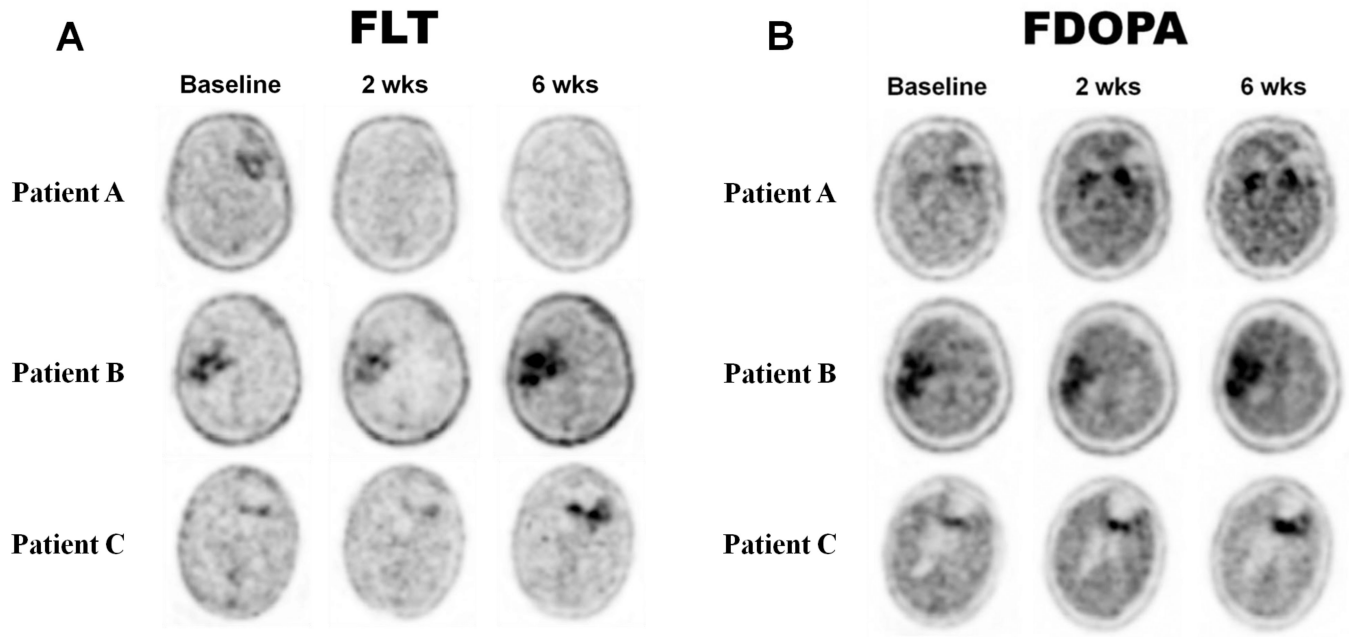


Figure 4.

(A) FLT PET images at baseline and after 2 and 6 weeks from the start of treatment as shown for a long-term survivor (Patient A, top row) and two short-term survivors (Patients B and C, middle and bottom rows). Images are displayed in radiological view, where the right side of the subject's brain is on the left side of the image and vice versa. (B) FDOPA PET images at baseline and after 2 and 6 weeks from the start of treatment as shown for a long-term survivor (Patient A, top row) and two short-term survivors (Patients B and C, middle and bottom rows). Note that Patient A has a tumor near the left striatum. Patients A, B, and C are Patients 20, 4, and 2 in Table 1, respectively.

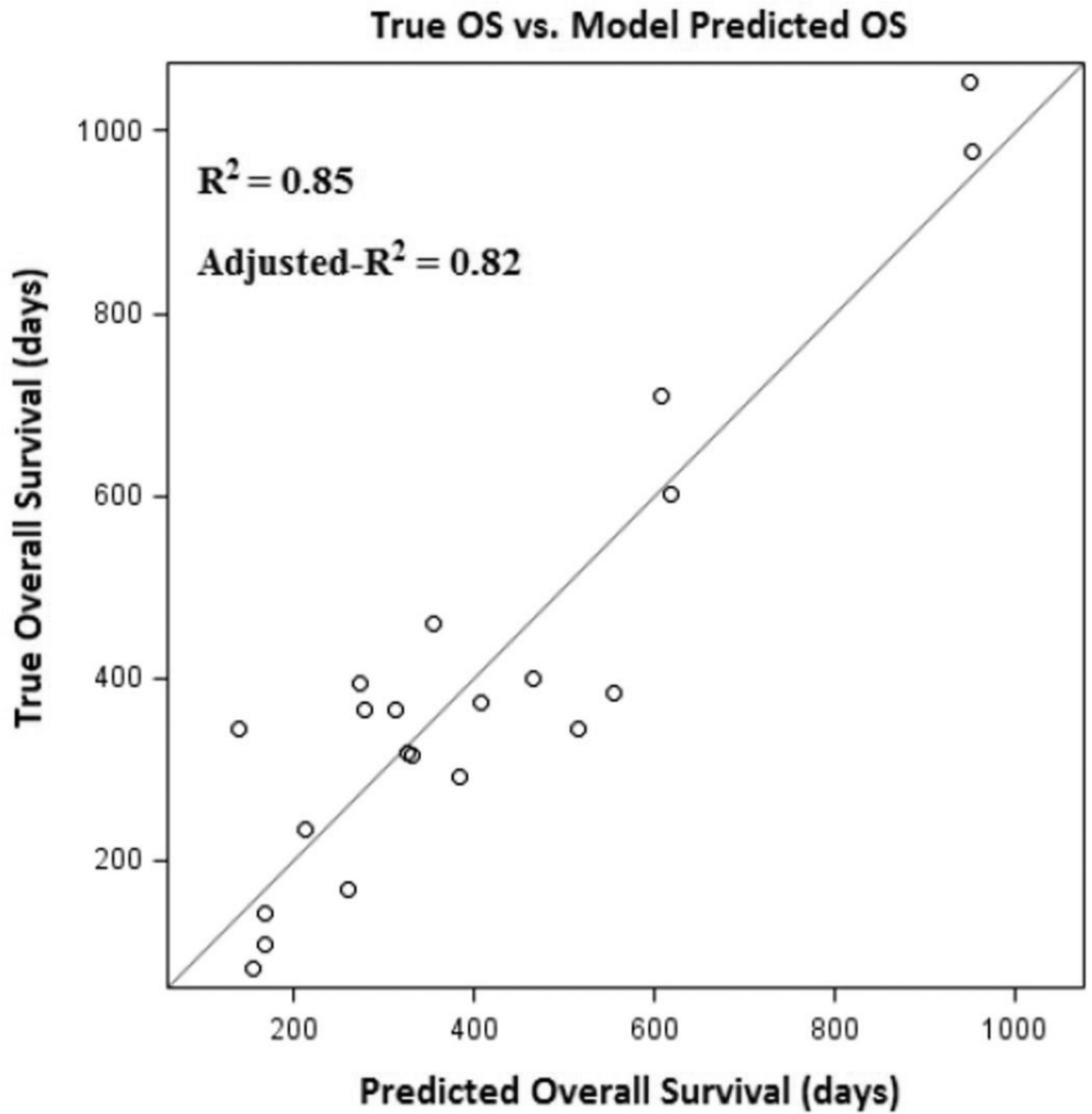


Figure 5.

Actual OS versus model predicted OS using only FLT kinetic information in the MLR analysis. Results from the best three-predictor MLR model are shown above.

Table 1

Clinical characteristics of patients

Patient No.	Sex	Age (y)	Pathology at Initial Diagnosis	Initial WHO grade	Pathology at recurrence	WHO grade at recurrence	Initial therapy	Prior treatments	Time from initial diagnosis (d)	PFS (d)	OS (d)
1	M	69	GBM	4	GBM	4	Chemotherapy/XRT	1	76	81	81
2	F	65	GBM	4	GBM	4	Chemotherapy/XRT	2	578	78	107
3	M	65	AA	3	AA	3	Chemotherapy/XRT	1	656	96	142
4	F	59	GBM	4	GBM	4	Chemotherapy/XRT	1	322	42	169
5	M	64	GBM	4	GBM	4	Chemotherapy/XRT	1	178	70	234
6	M	37	AA	3	GBM	4	Chemotherapy	2	4225	62	292
7	M	68	GBM	4	GBM	4	Chemotherapy/XRT	2	332	218	315
8	F	35	AA	3	GBM	4	XRT	3	2804	65	318
9	F	54	GBM	4	GBM	4	Chemotherapy/XRT	1	91	226	343
10	M	45	GBM	4	GBM	4	Chemotherapy/XRT	1	132	74	344
11	M	26	AA	3	GBM	4	Chemotherapy	3	462	96	364
12	F	40	GBM	4	GBM	4	Chemotherapy/XRT	1	462	44	366
13	F	47	GBM	4	GBM	4	Chemotherapy/XRT	1	160	176	374
14	M	68	GBM	4	GBM	4	Chemotherapy/XRT	1	488	343	383
15	F	70	GBM	4	GBM	4	Chemotherapy/XRT	1	362	184	395
16	F	61	GBM	4	GBM	4	Chemotherapy/XRT	2	719	137	400
17	F	37	GBM	4	GBM	4	Chemotherapy/XRT	1	126	304	460
18	M	57	GBM	4	GBM	4	Chemotherapy/XRT	1	1338	135	601
19	F	62	GBM	4	GBM	4	Chemotherapy/XRT	1	316	273	709
20	M	76	GBM	4	GBM	4	Chemotherapy/XRT	1	134	588	978
21	M	46	GBM	4	GBM	4	Chemotherapy/XRT	1	230	554	1054

* Time from initial diagnosis is the number of days from initial diagnosis to start of treatment in current study.

† GBM = glioblastoma multiforme; AA = anaplastic astrocytoma; XRT = radiation therapy.

Table 2

Multiple linear regression results using parameter information from FLT only, FDOPA only, and FLT and FDOPA combined.

Type of PET Information Inputted into a Three-Predictor Multiple Linear Regression Model	FLT only	FLT only	FLT and FDOPA
Kinetic Parameter Values at Each Study	Adjusted-R ² = 0.56	Adjusted-R ² = 0.32	Adjusted-R ² = 0.58
Change in Kinetic Parameter Values Between Studies	Adjusted-R ² = 0.80	Adjusted-R ² < 0.20	Adjusted-R ² = 0.83
Combination of Kinetic Parameter Values and their Changes	Adjusted-R ² = 0.82	Adjusted-R ² = 0.41	Adjusted-R ² = 0.83

Table 3

Parameter estimates from MLR model using information from FLT only (absolute values and changes).

Multiple Linear Regression Model for Predicting Overall Survival (MLR-1)		
Predictor Variable	Parameter Estimates	P-value
FLT V_d absolute value at S2	-443.29	<.0001
FLT k_4 ratio (S2/S1)	+158.44	<.0001
FLT k_2 ratio (S3/S2)	+289.66	<.0001
Intercept	+87.95	0.22

* $R^2 = 0.85$, adjusted- $R^2 = 0.82$, root MSE = 106 days, and the average variance inflation factors were 1.0.

S1 = Baseline FLT PET, S2 = FLT PET at 2 weeks after start of treatment, S3 = FLT PET at 6 weeks after start of treatment.